AD-A133 186 EXPERIMENTAL STUDIES OF SECONDARY ION EMISSION FROM WELL-CHARACTERIZED SURFACES(U) IRT CORP SAN DIEGO CA R L PALMER MAY 83 IRT-8213-002 AFOSR-TR-83-0747 1/1

UNCLASSIFIED F49620-81-C-0013 F/G 20/8 NL

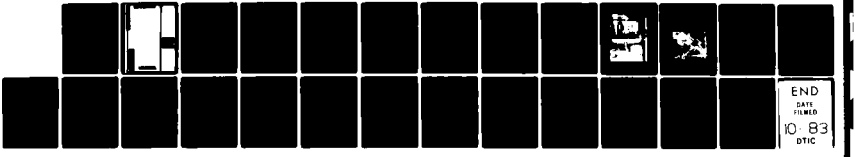

END
DATE FILMED
10-83
DTIC

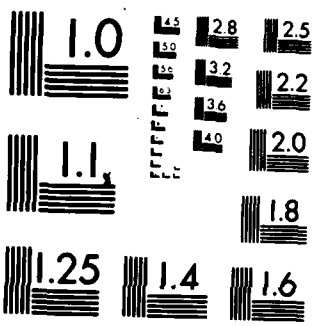

IRT 8213-002

EXPERIMENTAL STUDIES OF SECONDARY ION EMISSION FROM WELL-CHARACTERIZED SURFACES

Prepared by

R. L. Palmer

Prepared for

DEPARTMENT OF THE AIR FORCE
AIR FORCE OFFICE OF SCIENTIFIC RESEARCH
Bolling AFB, DC 20332

Under

Contract F49620-81-C-0013

May 1983

IRT Corporation

Instrumentation Research Technology

7650 Convoy Court • P.O. Box 80817
San Diego, California 92138

619 / 565-7171
Telex: 69-5412

UNCLASSIFIED

SECURITY CLASSIFICATION OF THIS PAGE (When Data Entered)

REPORT DOCUMENTATION PAGE	READ INSTRUCTIONS BEFORE COMPLETING FORM
1. REPORT NUMBER AFOSR-TR- 83-0747 Technical Report No. 2	2. GOVT ACCESSION NO. / 3. RECIPIENT'S CATALOG NUMBER
4. TITLE (and Subtitle) Experimental Studies of Secondary Ion Emission From Well-Characterized Surfaces	5. TYPE OF REPORT & PERIOD COVERED Interim
	6. PERFORMING ORG. REPORT NUMBER
7. AUTHOR(s) R.L. Palmer	8. CONTRACT OR GRANT NUMBER(s) F49620-81-C-0013
9. PERFORMING ORGANIZATION NAME AND ADDRESS IRT Corporation P.O. Box 80817 San Diego, California 92138	10. PROGRAM ELEMENT, PROJECT, TASK AREA & WORK UNIT NUMBERS 61102F 2301/A7
11. CONTROLLING OFFICE NAME AND ADDRESS Air Force Office of Scientific Research Building 410 Bolling AFB, DC 20332	12. REPORT DATE 31 May 1983
	13. NUMBER OF PAGES 23
14. MONITORING AGENCY NAME & ADDRESS(if different from Controlling Office)	15. SECURITY CLASS. (of this report) Unclassified
	15a. DECLASSIFICATION/DOWNGRADING SCHEDULE

16. DISTRIBUTION STATEMENT (of this Report)

Approved for Public Release; Distribution Unlimited

17. DISTRIBUTION STATEMENT (of the abstract entered in Block 20, if different from Report)

18. SUPPLEMENTARY NOTES

19. KEY WORDS (Continue on reverse side if necessary and identify by block number)

Secondary ion emission; tungsten; molybdenum; cesium; negative ions; surface ionization

20. ABSTRACT (Continue on reverse side if necessary and identify by block number)

The emission of ions from surfaces has been investigated using a specially constructed secondary-ion mass and energy analyzer. The energy spectra of $H^-(D^-)$ and $H^+(D^+)$ secondary ions produced by the impact of energetic incident ions such as H_1^+, H_2^+, H_3^+, Ar^+, and He^+ on polycrystalline molybdenum foil and single crystal W(110) have been measured. The secondary energy spectra and yield are relatively insensitive to the ion type and energy, but very sensitive to the physical-chemical state of the surface. In particular, the addition of cesium

DD FORM 1 JAN 73 1473 EDITION OF 1 NOV 65 IS OBSOLETE

increases the negative ion yield of molybdenum and tungsten by several orders of magnitude as well as shifting the energy distribution to lower energies. The spontaneous emission of H^- from W(110) was observed in an ambient of cesium vapor and hydrogen at temperatures above 600 K. The mechanism in this case appears to be surface chemi-ionization. The energy spectrum for this process is similar to that resulting from ion impact at low energies, but the surface chemi-ionization spectrum lacks the higher energy tail (E is less than 10 eV) characteristic of secondary ion emission.

TABLE OF CONTENTS

1. INTRODUCTION 1

2. EXPERIMENTAL FACILITIES 3

   2.1 SIMS Facility 3

3. RESULTS 9

   3.1 Molybdenum 9
   3.2 Tungsten 13

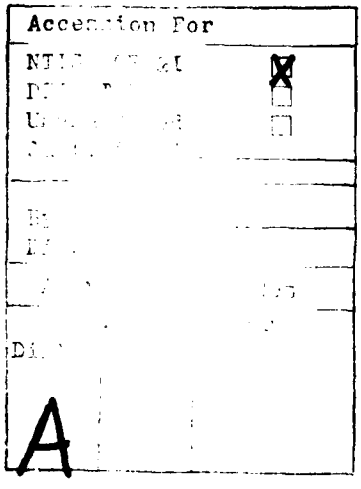

1. INTRODUCTION

Secondary ion emission from surfaces has been quite actively studied, both theoretically and experimentally. Secondary ion emission by ions (secondary ion mass spectrometry, SIMS), by electrons (electron stimulated desorption or ESD) and, to a lesser extent, photon stimulated desorption (PSD) have all been utilized to investigate surfaces, although there still remain significant fundamental questions regarding the mechanisms for all of these processes. Indeed, it appears unlikely that a predictive model of secondary ion emission from surfaces will soon be developed, although certainly some progress in that direction is being made. A crude but fairly successful theory of total sputtering yield (neutrals plus ions) has been developed by Sigmund (Ref. 1). However, the processes that give rise to secondary ions, or perhaps more properly, that lead to neutralization at the surface, are extremely sensitive to the details of the physical, chemical and electronic properties of the surface, and no comprehensive theory of ion emission currently exists. At this stage of development, experiments are needed that provide guidance for further development of the theory. To best serve this end, the experiments must be reduced to their simplest possible case, inasmuch as even an ideal surface is profoundly complicated, as compared with ion/molecule interactions in the gas phase, for example. A primitive state of theoretical development notwithstanding, secondary ion emission from surfaces will continue to increase in importance, because of its relevance to the operation of devices such as fusion reactors and ion sources.

One aspect of secondary ion emission that has received relatively less attention is negative ion emission from surfaces. Studies of negative ion emission will probably advance our understanding of positive ion emission as well, although the two phenomena are clearly different in important ways. On a practical level, there is growing interest in negative ions per se for applications in high energy tandem accelerators.

In this investigation, we have studied the emission of hydrogen ions including $H^-(D^-)$ and $H^+(D^+)$ from high purity molybdenum foil and single crystal W(110) surfaces. These surfaces were bombarded with energetic ions such as H^+, H_2^+, H_3^+, Ar^+ and He^+ at energies from 300 to 3000 eV, and secondary ion yield and energy spectra measured under a variety of surface chemical conditions including dosing with cesium.

The spontaneous emission of H^- ions was also observed under certain conditions in the absence of energetic ion irradiation. The mechanism of this process appears to be surface chemi-ionization to form H^- during the chemisorption of cesium and hydrogenic species on a heated surface. This process may offer a promising approach to the design of a practical, high-brightness H^- source.

2. EXPERIMENTAL FACILITIES

2.1 SIMS FACILITY

The apparatus used for these studies is the secondary ion mass spectrometer (SIMS) facility constructed at IRT. An external view of this apparatus is given in Figure 1. Figure 2 presents a schematic view of this same apparatus showing the ion source, magnetic charge-to-mass ratio analyzer, and SIMS detector. The ion source is capable of giving stable ion currents of up to approximately 1 μa at energies from 300 eV to 75 keV. The ion beam spot size on the target is about 1-mm radius, allowing high collection efficiency and sharp focusing of the secondary ions.

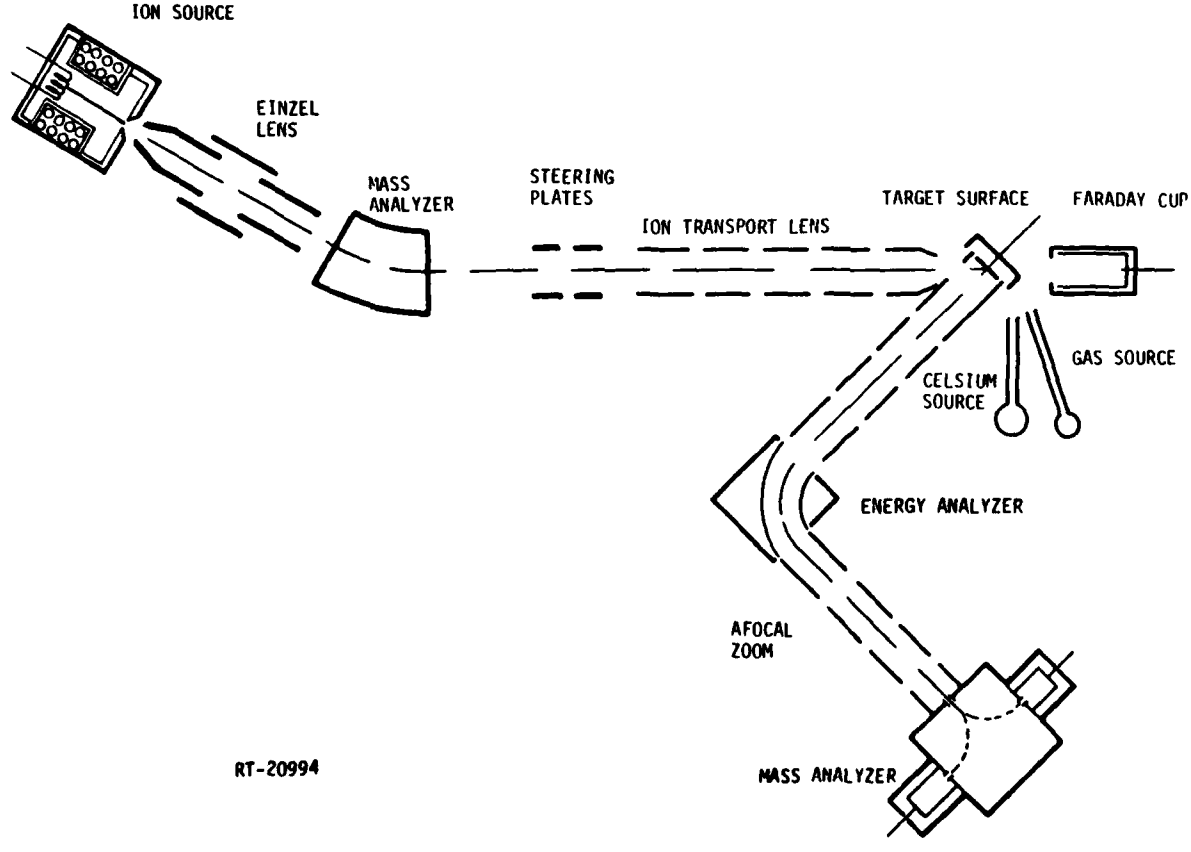

Figure 1. Secondary ion mass spectrometer showing ion source, bending magnet, and target chamber

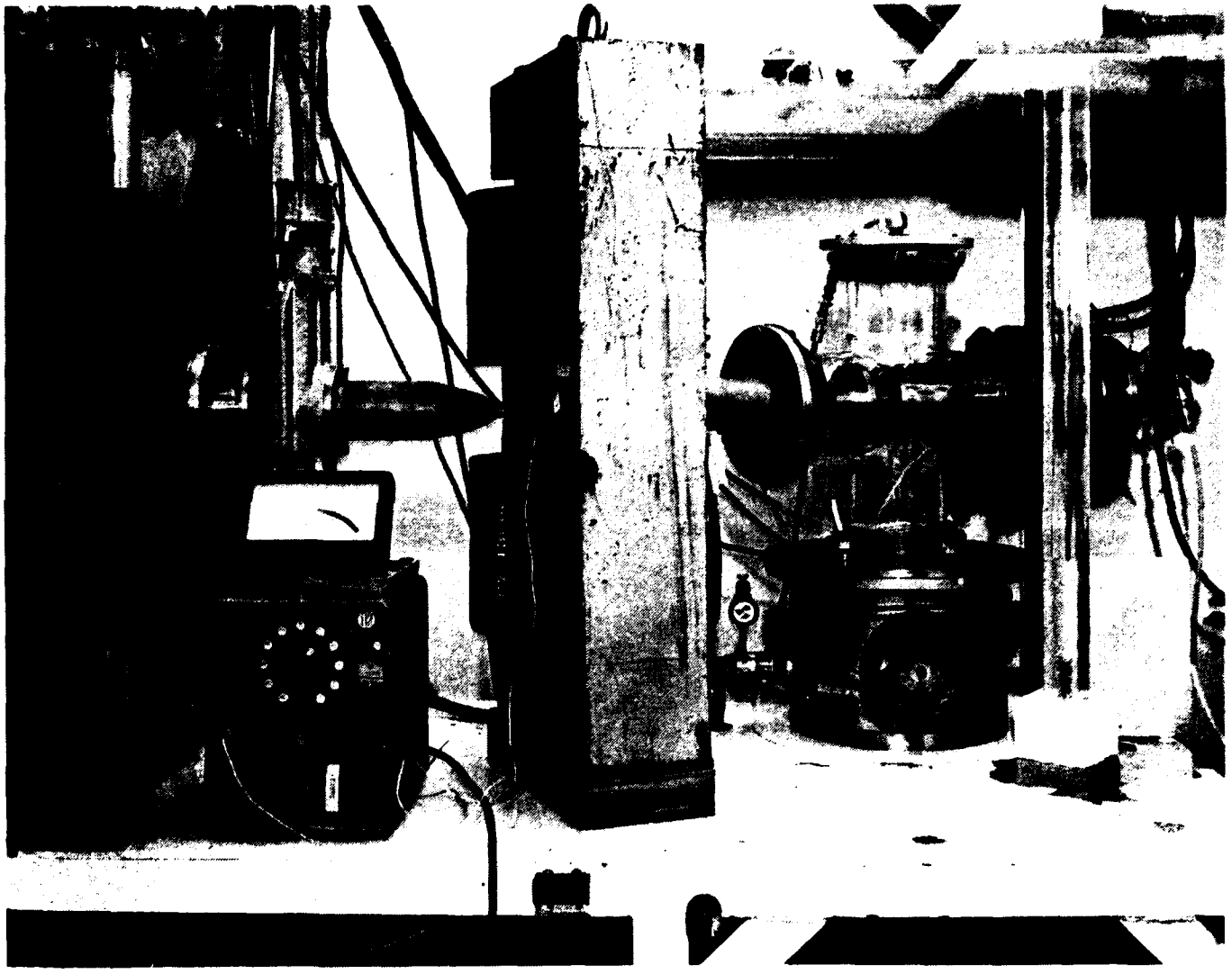

Figure 2. Ion source and secondary ion mass spectrometer

A close-up view of the detector assembly as seen from above is shown in Figure 3. The SIMS detector consists of a high collection efficiency focusing lens assembly followed by an electrostatic hemispherical energy analyzer which bends the ions through 90°. An electrostatic afocal zoom lens assembly focuses the energy selected ions into a magnetic-type mass analyzer. Both the energy and mass resolution of the SIMS detector can be varied independently in situ by means of externally adjustable knife-edge slits.

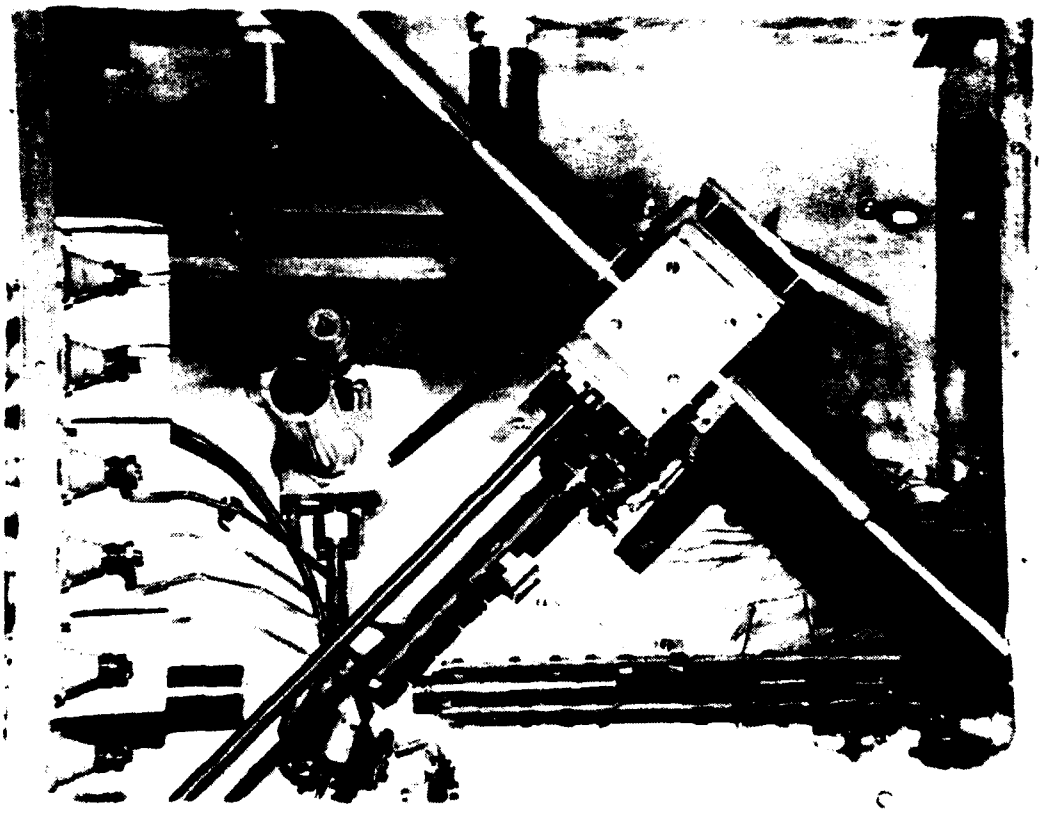

Figure 3. Secondary ion mass spectrometer detector assembly including target and cesium source

A cesium vapor source and gas dosing cell are also seen adjacent to the target in Figure 3. The target is shown rotated away from the SIMS extractor lens as it would be to allow direct cesium dosing of the target surface. Additionally, the target assembly includes a tungsten filament located directly behind the target so that the target may be heated, either by radiation or to higher temperatures by electron bombardment. The capability of going to high temperatures is important for the cleaning of bulk refractory targets such as molybdenum, tantalum, and tungsten. In addition to high temperature heating, target surfaces can also be cleaned by sputter etching with 1-5 keV Ar^+ using the SIMS ion source described above.

The detector assembly resides in a stainless steel box which forms a secondary vacuum chamber that is pumped using the titanium filament seen in the upper left of Figure 3. A nude ion gauge, lower right, is used to monitor the pressure inside the box. After extensive bake-out, the pressure inside the box can be brought down to the low 10^{-9} torr regime, about a factor of ten lower than the main chamber outside the box.

Primary ions enter the box through a small hole located in the lower right hand corner of Figure 3, just under the ion gauge. A combination of lenses and steering plates extending in a straight line down from this hole focuses the ion beam through a hole at the end of the collector lens assembly. When the target is swung out of the way, the primary ion current can be measured directly using the Faraday cup located in the lower left-hand corner of the figure.

The extraction lens assembly is set at forty-five degrees to the incident ion beam and focuses the point of emission on the target surface at the entrance to the 90° hemispherical energy analyzer. In Figure 3, the analyzed ions are bent vertically (out of the page) up into the mass analyzer. Positive ions are bent to the left (looking down) and negative ions to the right where they are collected in Faraday cup detectors. The ion currents are measured directly using a Keithley Model 602 Electrometer. The entire detector assembly is nonmagnetic and the mass and energy analyzers are gold-plated to improve resolution.

The secondary ion energy and mass analyzer electrostatic lens optics were designed for maximum collection efficiency. The primary beam passes through a small hole in the first extraction lens and strikes the target at 45° when the target is in the measurement position at the entrance of the extraction lens system. The extraction lens produces an electric field pattern that pulls ions from the target and focuses them into a beam whose axis is normal to the target surface with a focal point at the entrance focal point of the electrostatic hemispherical energy analyzer. Since the

usual electrostatic lens formulae are not applicable to the extraction region, electron models of this lens system were constructed and tested, the focal spot being observed on a glass screen coated with cathode ray tube phosphor. The target was simulated by a plate with an oxide-coated cathode mounted flush in a hole in its center. The cathode diameter was somewhat larger than the beam spot on the target in the finished apparatus. Several lens geometries were tested under a variety of focusing conditions until one was found which could consistently produce a small focal spot. Current measurements were performed which demonstrated that all of the electrons emitted from the cathode landed on the focal spot (none of them went astray, landing on electrode surfaces, etc.). The energy analyzer is a 90° spherical deflector which has excellent transmission characteristics due to its inherently large acceptance angle. The exit focus of the analyzer is imaged at the analyzer exit slit by an afocal zoom electrostatic lens whose purpose is explained below. This slit is also the entrance focal point of a 90° deflection permanent magnet mass spectrometer. The mass spectrometer has two exit slits and two ion collectors on opposite sides so that it can collect equally well both positive and negative ions. The energy analyzer and mass spectrometer deflect the ion beam in orthogonal planes.

A permanent magnet-type mass spectrometer was used because of its compactness, simplicity, and ultra-high vacuum compatibility. Its relatively weak magnetic field strength does, however, limit its use to species of low mass such as the isotopes of hydrogen for which it was intended. The afocal electrostatic zoom lens has the favorable property of maintaining a constant distance between focal points and nearly constant magnification over a wide range of acceleration ratios. (The magnification, m varies as $R^{\frac{1}{4}}$ where R is the ratio of incoming to outgoing beam energy.)

The slit (1) at the exit of the energy analyzer and entrance of the mass spectrometer, and the slits (2) at the exits of the mass spectrometer are adjustable from outside the vacuum wall. This permits the energy resolution and mass resolution of the instrument to be varied independently during an experiment. With the slits fully opened, the collection efficiency is approximately 100 percent, at least for thermal energy electrons. This was determined using a heated cathode in place of the target as described above.

Ion energy spectra using this instrument are obtained in the following way. The potential between the hemispheres of the 90° analyzer is set to pass ions of a convenient energy, say 20 eV. (The design potential is 16/15 E_i, where E_i is the ion energy or 21.33 V in this case.) The target potential is then lowered, starting nominally

from 20 V with respect to the analyzer to sweep the energy spectrum. In principle, for a target potential of 20 V with respect to the analyzer, only ions ejected with zero kinetic energy can pass through the 90° hemispheres. In practice, however, there is typically a contact potential difference of up to 5 V between the target and the gold-plated analyzer. This contact potential difference, arising from the different work functions of the gold and clean or cesiated-molybdenum and tungsten surfaces, produces a corresponding shift in the measured ion spectra. This shift is toward higher measured energies for positive ions and toward lower energies for negative ions, as can be seen in the experimental results presented in the following section. A comparison of positive and negative ion spectra, therefore, fortuitously provides a crude measure of the target surface contact potential relative to gold.

3. RESULTS

3.1 MOLYBDENUM

In Figure 4 are presented the measured energy spectra of H^+ and H^- ions ejected from a cesiated-molybdenum surface by 1500 eV H_2^+ incident ions. The molybdenum used was five nine's purity polycrystalline foil. All of the spectra reported here were taken with the energy analyzer adjusted for maximum resolution. The primary ion beam, H_2^+ in this case, was incident on the target at 45^o at a current of 10^{-5}–10^{-4} ampere-cm^2. The hemispherical energy analyzer was set to nominally pass 50 eV (singly-charged) particles. The energy scales in Figures 4 through 8 are based on the applied potential between the target and analyzer relative to the 50 eV energy pass of the energy analyzer, i.e., zero on the energy scale corresponds to a target potential of -50 V with respect to the analyzer, +10 eV is -40 V and so on. The obvious instrumental shift of the two spectra due to the contact potential between the cesiated molybdenum target and gold-plated analyzer, and the position of the spectra on a true energy scale is discussed in Section 4.

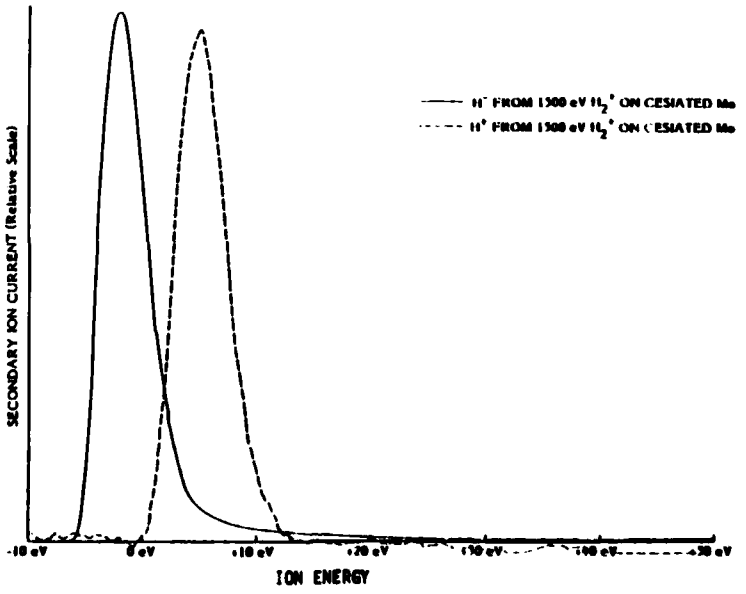

Figure 4.

The molybdenum target was periodically cleaned in situ by flashing to 2000 K and sputtering with the primary ion beam, a process which, of course, also necessarily accompanies measurements of the secondary ion spectra. After cooling to around room temperature, the target was dosed with cesium from a stainless steel valve that was first heated and then opened for a period of time (approximately 30 seconds) sufficient to deposit several monolayers on the surface. Although no direct measurement of the surface condition could be made in the present study, it is known that at about one quarter of a monolayer, cesium forms a surface structure on molybdenum that is stable up to about 650 K. This appears to be true in our case as well, because flashes to higher temperatures were required to cause an irreversible change in the secondary ion yield.

Figure 5 presents results for the H^- secondary energy spectra taken under conditions similar to Figure 2, but with the secondary extraction field (first lens) set for (a) maximum collected ion current, and (b) at the same potential as the target. The collected ion current in case (b) was a factor of 25 less than the maximum current with the first lens 60 V positive with respect to the target. The only difference in the two curves is an expected loss of very low energy ions with zero extraction field.

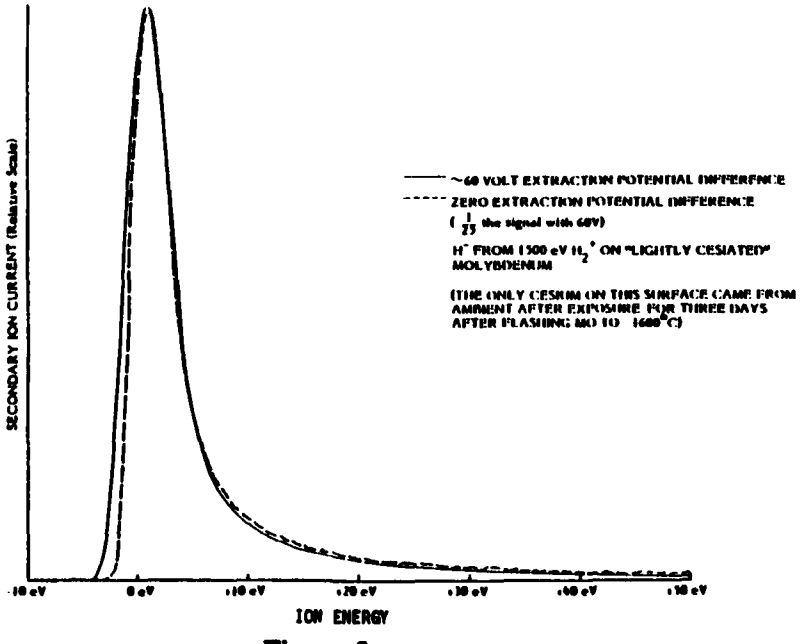

Figure 5.

Figure 6 compares the energy distribution and yields of H^- ions for three incident ion species, H^+, H_2^+ and H_3^+. The major difference in comparing these results is in the total yields (measured with the aperture slits full open) although there is also a small systematic change in the yields at higher energies.

Figure 7 compares the yields of H^- vs energy with H_2^+ ions incident at energies of 750, 1500, and 3000 eV. Again, the major difference appears in the total yield with a trend toward less high energy ejection of H^- as the incident ion energy is increased. A comparison of the H^- spectrum for 1500 eV incidence H_2^+ with the equivalent data in Figure 4 indicates the typical variation in yield and energy distribution that were observed when these measurements were repeated under nominally the same conditions.

Figure 8 gives results using an incident Ar^+ beam at 1500 eV and 750 eV, with and without an added H_2 ambient. Both the total yields and energy distributions are qualitatively very similar to the results using incident hydrogenic ions. The secondary H^- yield could be significantly increased by raising the ambient H_2 pressure suggesting that this is the source of hydrogen for the secondary ion emission with incident Ar^+ and incident hydrogen ions as well.

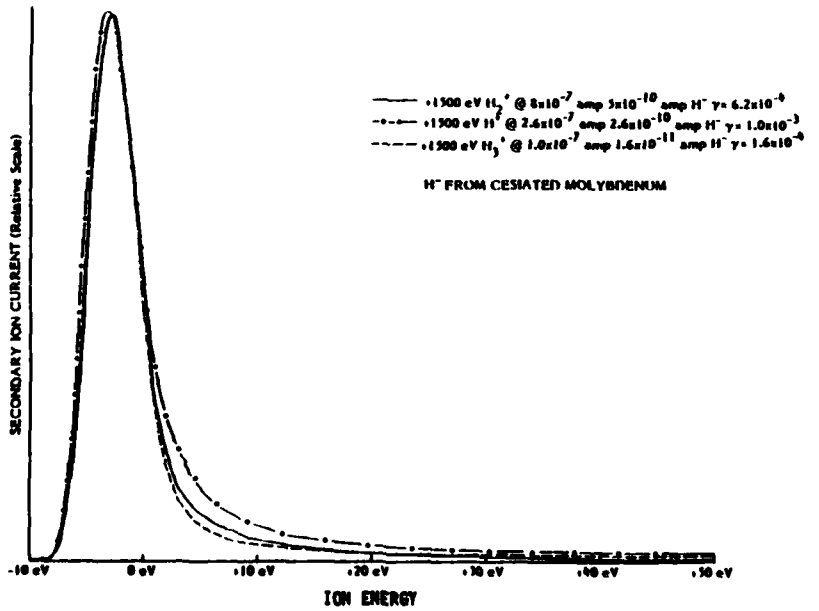

Figure 6.

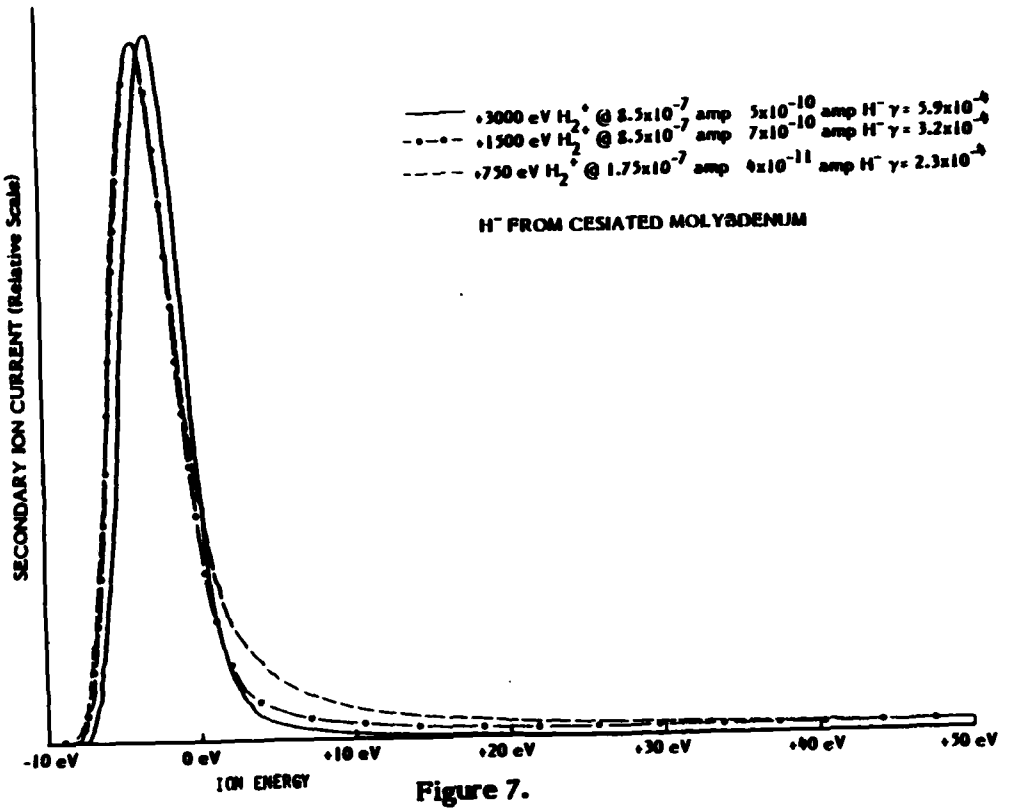

Figure 7.

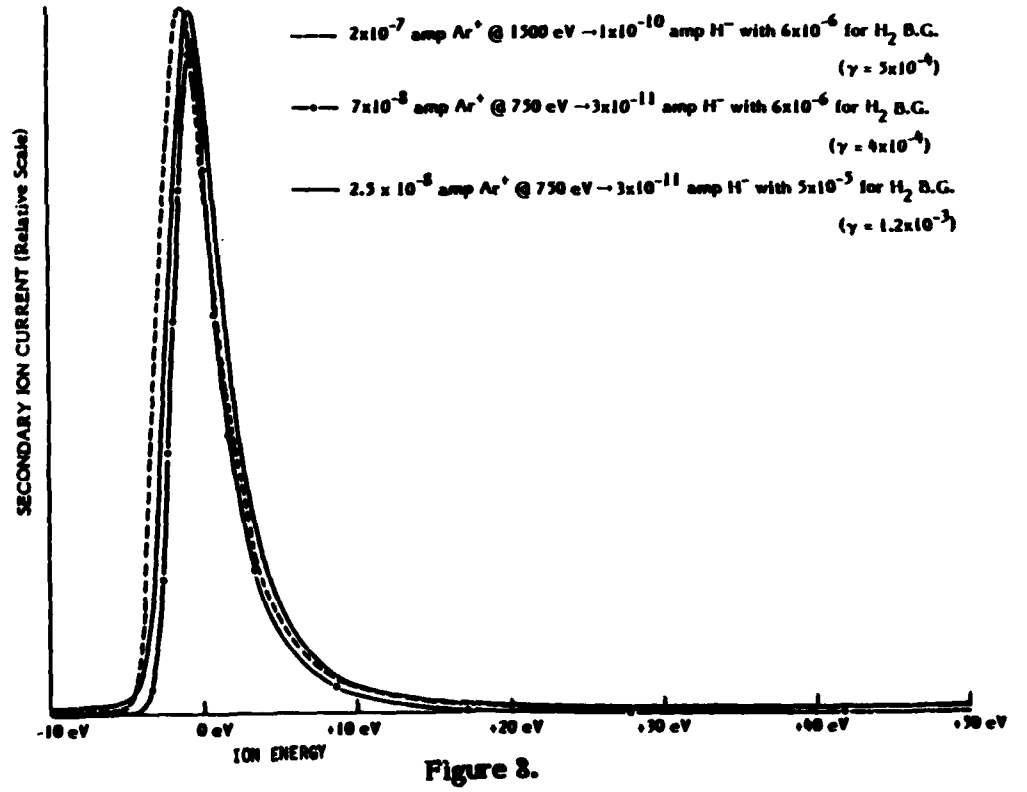

Figure 8.

Several important general observations were also made during the course of these measurements. First, the secondary H^- current, when the target was first exposed to the incident ion beam, was an order of magnitude greater than the steady-state current. Deflection of the beam to a different spot on the surface also produced a smaller, temporary increase in secondary ion yield that decayed within a few seconds, to a relatively stable yield that held essentially constant for periods of hours, even though the incident ion current density was quite high (equal to or greater than 10^{-4} ampere-cm^2). This result was very surprising considering the expected removal of molybdenum, cesium, and other surface species through the sputtering action of energetic incident ions.

The secondary ion yield for H^- was immeasurably small ($\gamma \leq 10^{-8}$) on the molybdenum surface immediately after flashing to 2000 K and cooling to room temperature. If the temperature-cycled surface was allowed to age in the vacuum ambient for several hours, including overnight when the vacuum pumps were off, the ion yield would increase to easily measurable values. When the freshly temperature-cycled molybdenum surface was dosed with cesium, the secondary H^- yield went immediately to near the maximum observed values. Aging of the cesiated molybdenum tended to further increase the yield by as much as an order of magnitude, this change occurring over a period of many hours or days. The yield also about doubled when the target was heated to 500 K. No significant changes in the shape of the energy distribution accompanied these changes, however, although for very low overall yields the high energy tail becomes more predominant relative to the low-energy peak. Interestingly, an H^+ secondary ion current was never observed under conditions where H^- was not observed and always to a significantly lesser degree (typically about two orders of magnitude below the H^- current). Finally, although the energy data given in Figures 4 through 8 terminates at 50 eV, measurements were often made up to the energy of the incident beam and no increase in yield at higher energies was ever observed.

3.2 TUNGSTEN

For these experiments, the polycrystalline molybdenum foil was replaced with a tungsten single crystal oriented with the (110) planes parallel to the surface. Before installing this crystal in the SIMS apparatus, it was cleaned in UHV by heating to high temperatures ($\leq$ 3000 K) and sputtering with Argon ions. The final cleanliness of the surface was verified by Auger electron spectroscopy (AES) and the orientation verified

using low energy electron diffraction (LEED). The W(110) crystal was then transferred to the SIMS chamber for study.

In the SIMS apparatus, the W(110) crystal was bombarded with 900 eV Ar^+ ions and its temperature raised to 1600 K to remove surface contamination. The vacuum level at this time was in the low 10^{-6} torr region. As the crystal cooled, secondary H^- emission was observed. The energy dependence of this emission current was measured, as described previously. Spectra corresponding to crystal temperatures of 300 and 560 K are presented in Figure 9. These spectra exhibit an unusual double peak structure, as compared with previous spectra, that persisted during moderate temperature cycling. Because of the relatively poor vacuum conditions (10^{-6} torr) during these measurements, the surface cannot be considered "clean," but these spectra do suggest some interesting facts. First, the sharpness of the features (note the expanded energy scale in Figure 9) indicate that the resolution of the energy analyzer is about 1 eV or better. Secondly, the significantly greater reduction in the higher energy (3.75 eV) peak at 580 K suggests that we are observing H^- emission from two distinct chemical binding states, the higher energy peak being less strongly bound and, therefore, depopulating more rapidly as the target temperature is raised. (This high energy peak disappeared completely at a slightly higher temperature.) The observed energy separation between these two sharp peaks is undoubtedly the result of a characteristic difference in the local work function of the two binding states, the higher energy state indicative of a work function that is about 2.5 V greater. Adding H_2 gas to the target chamber caused an increase in the overall H^- emission, but did not change to the shape of the H^- spectrum. Since a large fraction of the ambient gas is H_2, along with H_2O and CO, it is presumed that residual H_2 gas provided the source of the surface hydrogen for the H^- emission. The addition of H_2O and other hydrogenic gases, such as C_2H_2, did not increase the H^- yield.

Following these initial experiments, the SIMS chamber was baked and, over a period of several days, the vacuum ambient decreased into the 10^{-9} torr regime. During this time, the energy spectra for H^- secondaries gradually lost its two component nature and became a single peaked distribution qualitatively similar to those previously seen on molybdenum. One such spectrum for H^- from room temperature W(110) is shown in Figure 10. Also shown is the corresponding H^+ distribution under the same conditions. For these data, the target was irradiated with 600 eV He^+ ions at a current of 1×10^{-8} amperes (approximately 1×10^{-6} amperes/cm^2). With He^+ irradiation at this energy and this current or lower, the secondary emission did not

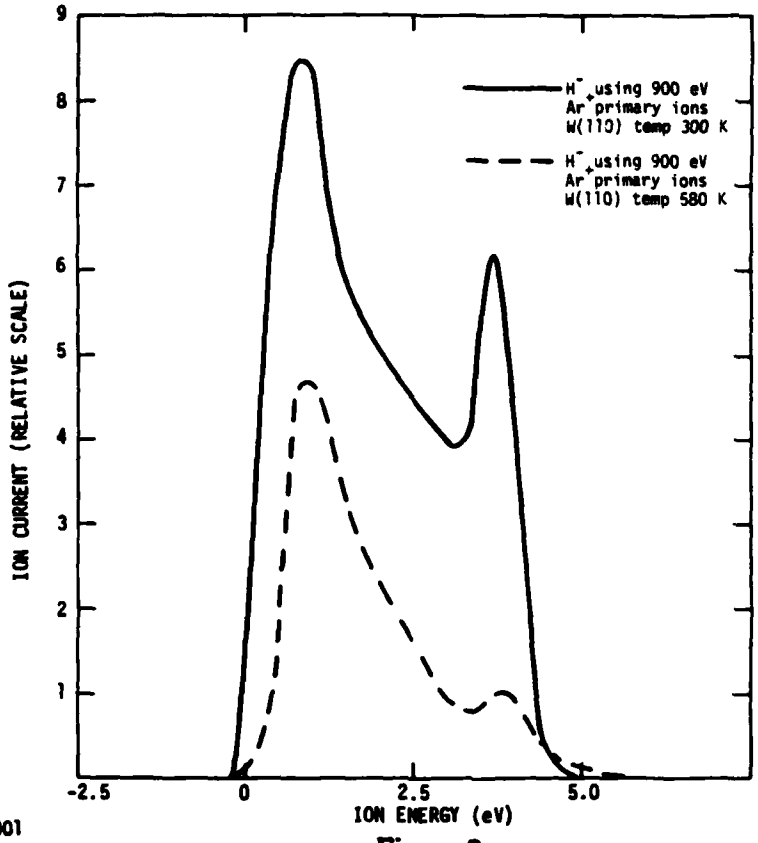

RT 24001

Figure 9.

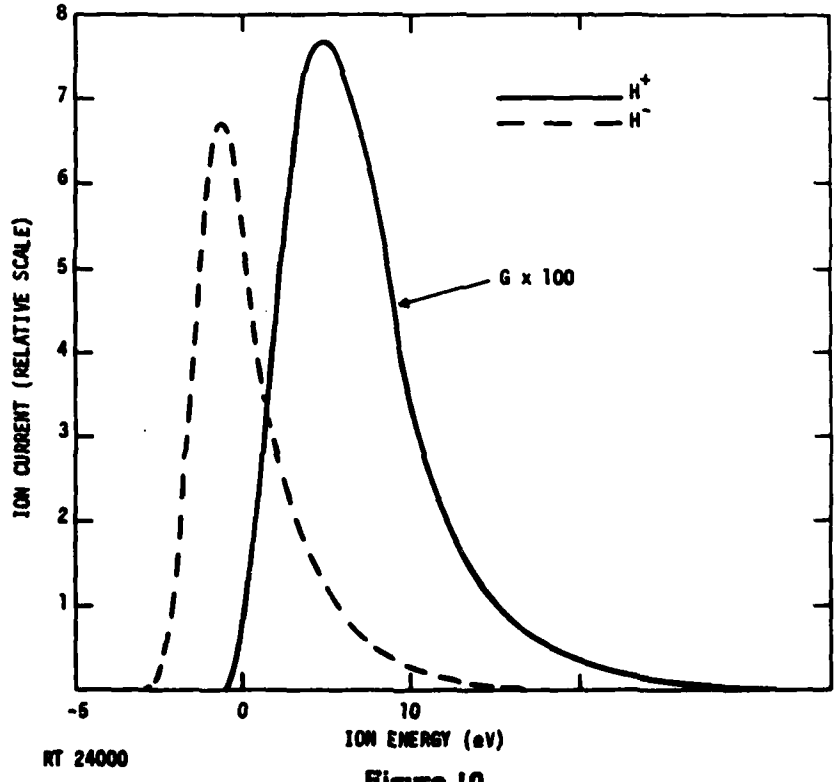

RT 24000

Figure 10.

change measurably during the measurements; i.e., a quasi-static surface condition existed. However, the effect of higher incident-beam currents is significant at low ambient pressures ($\leq 10^{-8}$), as can be seen in Figure 11. Here, the H^- energy spectra are compared at two primary ion currents 1×10^{-8} and 4×10^{-8} amperes. At the higher current, the H^- secondary current (although initially a factor of four higher) gradually diminshed until it reached a steady value that was approximately 1/4 the inital value. Apparently, the surface hydrogen coverage has been reduced by 1/16 by the sputtering action of the primary beam. The H^- spectrum under these conditions is significantly broader, and the low-energy peak is suppressed relative to the high-enrgy tail. This same effect is achieved by heating the crystal which also reduces the surface hydrogen coverage.

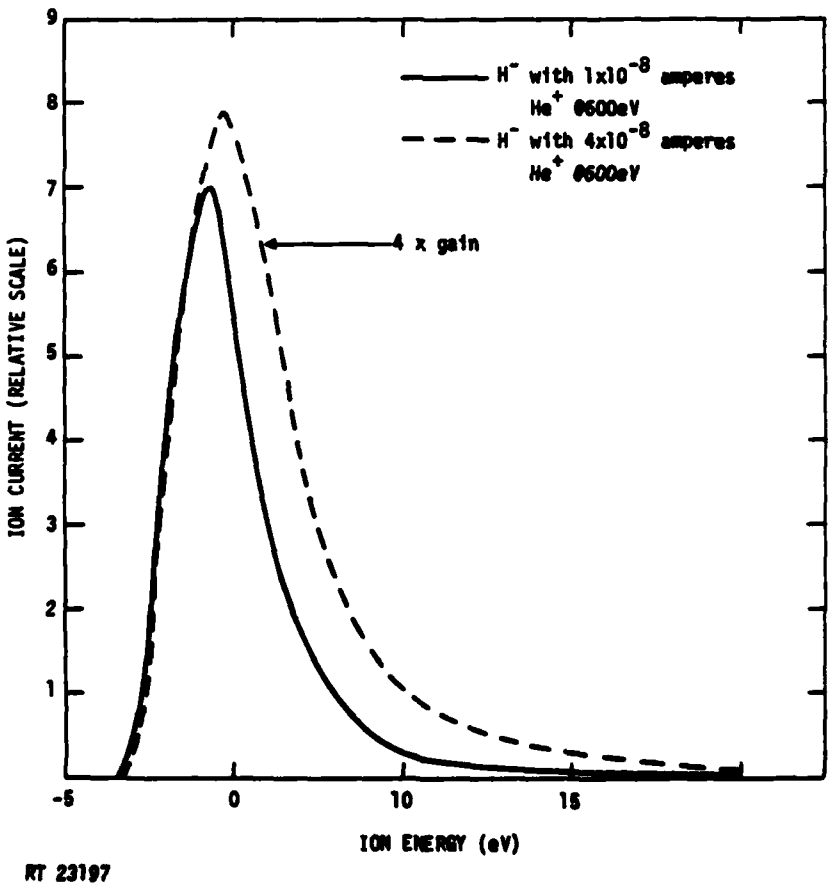

Figure 11.

A noteworthy trend in the H^- spectra of Figures 9 through 11 is the gradual shift in the zero to the left; i.e., an apparent decrease in the work function of the W(110) crystal of about 2.5 eV. This is suggestive of some contamination of the target, possibly by traces of cesium left in the chamber from previous experiments. Therefore, the SIMS spectrometer, including the surrounding vacuum box, was removed and cleaned thoroughly with soapy water followed by distilled water and finally alcohol. After drying, the apparatus was reinstalled in the vacuum chamber. The entire SIMS box was again baked out and the base pressure gradually reduced to the 10^{-9} torr regime. The W(110) target was also baked for extended periods (hours) at temperatures up to 1800 K. After this procedure, some significant differences were observed. Qualitatively, the H^- and H^+ yields were greatly reduced and the spectra were shifted back to near zero on the energy scale. Immediately after flashing the target to 1800 K and cooling to near room temperature, no secondary ion emission could be detected. After a period of a few minutes, the H^- signal became measurable. However, the addition of up to 10^{-5} torr of H_2 gas did not affect this recovery rate as had been noted earlier. Evidently, the previous results had been affected by some type of contaminant such as cesium. An H^- spectrum taken 15 minutes after flashing the target to 1800 K is shown in Figure 12 (solid curve). This spectrum is presumed to approach most closely the "clean" surface condition, although from the cleanest surface no secondary ion emission is observed. Next, the W(110) crystal was dosed with cesium by opening the valve to the heated cesium cell. After cesiating, the dashed spectrum in Figure 12 was obtained. The secondary ion yield, γ, increased to about 1×10^{-3} for 600 eV He^+ ions, and shifted about 4.5 eV to the left; i.e., indicating a lower work function.

During the course of these experiements, both on molybdenum and tungsten, several attempts were made to obtain a spectrum of thermal ions to determine both the zero energy and resolution of the analyzer. This was done by turning off the primary ion beam and heating the target. Aithough some small currents were observed, they had not been steady enough to obtain an accurate spectrum. However, after cesiating the W(110) crystal, an easily measurable H^- emission was seen, with no primary ion beam, when the crystal was heated moderately. This H^- emission current increased as more cesium was added to the spectrometer box, and the ambient temperature was raised to increase the cesium partial pressure. The addition of hydrogen or water to the vacuum ambient also caused a further increase in the H^- emission. To verify that these ions were indeed coming from the target, several tests were performed, including rotating the target away from the collection lens and turning off the target heater and

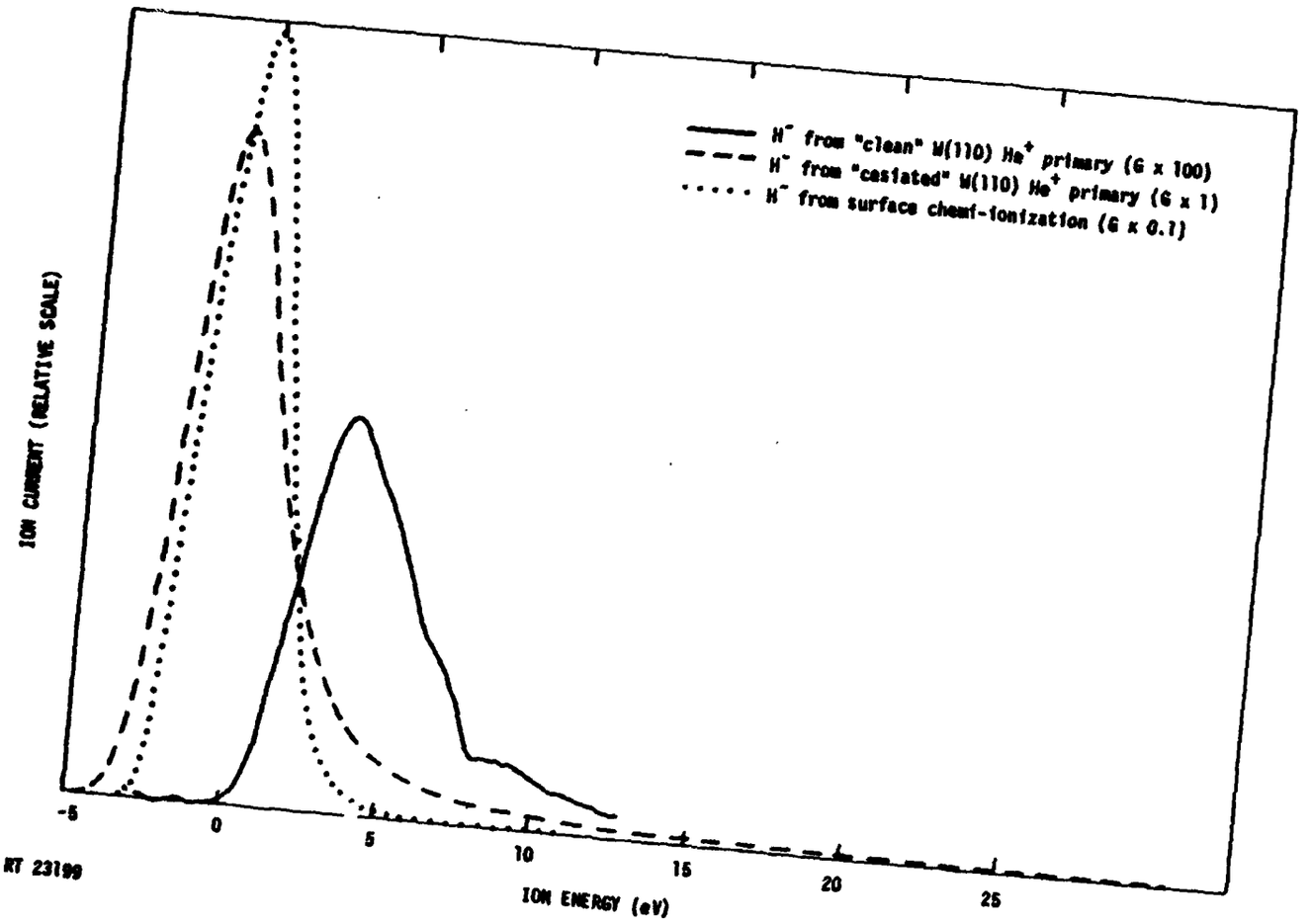
H⁻ from "clean" W(110) He⁺ primary (G x 100)
H⁻ from "cesiated" W(110) He⁺ primary (G x 1)
H⁻ from surface chemi-ionization (G x 0.1)
ION CURRENT (RELATIVE SCALE)
-5
0
5
10
15
20
25
ION ENERGY (eV)
RT 23199

Figure 12.

ion gauge filament. All of these tests verified the source of these ions as the W(110) surface. The measured energy spectrum of these ions, taken at a surface temperature of 650 K, is shown in Figure 12 (dotted curve). It is slightly more narrow than the spectrum of H^- produced by He^+, and the high energy tail is absent. If this ion emission has a Boltzmann energy distribution at the temperature of the surface, then the true energy spectrum is only a few tenths of a Volt wide. Evidently these H^- ions are not truly thermal and/or there is a range of local work functions on the surface. Further evidence as to the nature of this H^- emission is given by the surface temperature dependences shown in Figure 13. Here, the H^- emission during a heating and cooling cycle in the presence of cesium and water vapor is shown. The heating and cooling rates were approximately 10 $Ksec^{-1}$. The cooling curve was quite reproducible when the W(110) crystal was first raised to 1100 K or higher, whereas the heating cycle varied considerably from one cycle to the next. These results suggest that the H^- emission arises from the chemical interaction of gaseous species with the "clean" W(110) surface. This complicated chemical interaction evidently involves cesium and hydrogenic species such as H_2 and H_2O. This phenomenon warrants further study inasmuch as it appears to provide a simple means of generating large currents of low-energy H^- ions.

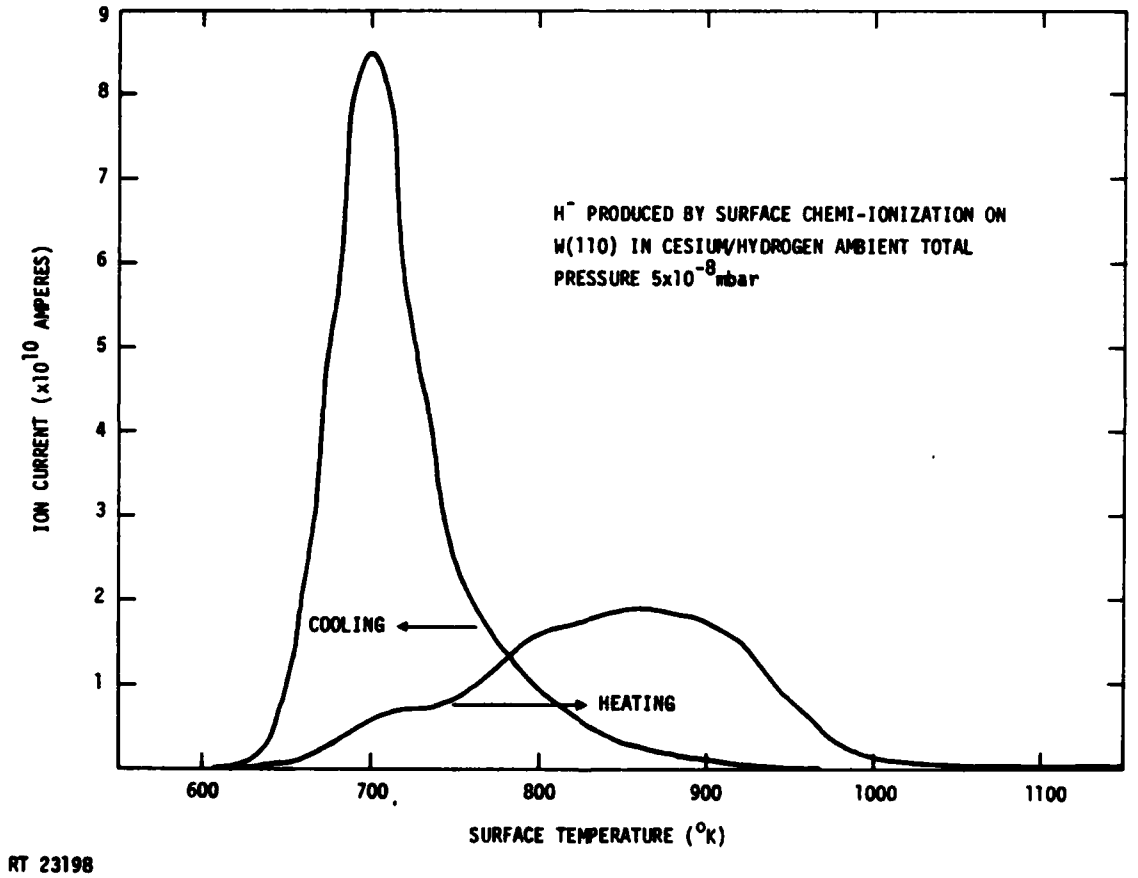
H⁻ PRODUCED BY SURFACE CHEMI-IONIZATION ON
W(110) IN CESIUM/HYDROGEN AMBIENT TOTAL
PRESSURE 5x10⁻⁸mbar
COOLING
HEATING
ION CURRENT (x10¹⁰ AMPERES)
SURFACE TEMPERATURE (°K)
9
8
7
6
5
4
3
2
1
600
700
800
900
1000
1100
RT 23198

Figure 13.


DATE
ILME